



OPEN

Fluorine-based color centers in diamond

S. Ditalia Tchernij^{1,2,3}, T. Lühmann⁴, E. Corte^{1,2}, F. Sardi¹, F. Picollo^{1,2}, P. Traina³, M. Brajković⁵, A. Crnjac⁵, S. Pezzagna⁴, Ž. Pastuović⁶, I. P. Degiovanni^{3,2}, E. Moreva³, P. Aprà^{1,2}, P. Olivero^{1,2,3}, Z. Siketić⁵, J. Meijer⁴, M. Genovese^{3,2} & J. Forneris^{1,2,3}✉

We report on the creation and characterization of the luminescence properties of high-purity diamond substrates upon F ion implantation and subsequent thermal annealing. Their room-temperature photoluminescence emission consists of a weak emission line at 558 nm and of intense bands in the 600–750 nm spectral range. Characterization at liquid He temperature reveals the presence of a structured set of lines in the 600–670 nm spectral range. We discuss the dependence of the emission properties of F-related optical centers on different experimental parameters such as the operating temperature and the excitation wavelength. The correlation of the emission intensity with F implantation fluence, and the exclusive observation of the afore-mentioned spectral features in F-implanted and annealed samples provides a strong indication that the observed emission features are related to a stable F-containing defective complex in the diamond lattice.

Diamond has been widely investigated as an appealing material for quantum optics and quantum information processing applications, due to the availability of several classes of optically active defects (usually referred to as “color centers”) that can be suitably engineered in its crystal structure^{1–3}. To date, the most prominent type of defect is the so-called negatively-charged nitrogen-vacancy center (NV⁻), due to several key features of this system, namely: photo-stability at room temperature, high quantum efficiency and most importantly unique spin properties with great potential for applications in quantum sensing and computing^{4–9}.

The need for single-photon emitters displaying desirable opto-physical properties (high emission rate, narrow linewidth) has also motivated the discovery and characterization of several classes of optical centers in diamond alternative to the NV complex, based (among others) on group-IV impurities¹⁰ (Si^{11,12}, Ge^{13,14}, Sn^{15,16}, Pb^{17,18}) and noble gases (He, Xe^{19–21}). In this context, ion implantation represents a powerful and versatile tool to engineer a broad range of different types of color centers, allowing for the fine control of key parameters such as ion species and energy, as well as irradiation fluence to determine the type and density of defect complexes^{22,23}.

Up to now though, the number of the emitters characterized by a reproducible fabrication process is fairly limited, and a systematic investigation in this field is still to be finalized. Thus, the fabrication of novel luminescent defects with desirable properties upon the implantation of selected ion species still represents a crucial strategy to achieve further advances in the field. Following from a previous report with preliminary results on this system²⁴, in this work we report on the systematic characterization in photoluminescence (PL) under different optical excitation wavelengths of F-related color centers in diamond created upon ion implantation and subsequent annealing.

Experimental

The characterization of F-related emission here presented was performed on a type-IIa single-crystal diamond sample (*Sample #1*) produced by ElementSix with Chemical Vapor Deposition technique, namely a 2 × 2 × 0.5 mm³ “electronic grade” substrate having nominal concentrations of both substitutional nitrogen and boron impurities below the 5 ppb level.

The sample was implanted with 50 keV F⁻ ions at the low-energy accelerator of the University of Leipzig. Several circular regions of ~ 175 μm diameter were irradiated at varying fluences in the 5 × 10¹⁰–5 × 10¹⁵ cm⁻² range by the use of a custom beam collimator. An additional region was implanted with 1.47 MeV F²⁺ ions (1 × 10¹³ cm⁻² fluence) at the Laboratory for Ion Beam Interactions of the Ruđer Bošković Institute. The sample

¹Physics Department, University of Torino, 10125 Turin, Italy. ²Istituto Nazionale Di Fisica Nucleare (INFN), Sezione Di Torino, 10125 Turin, Italy. ³Istituto Nazionale Di Ricerca Metrologica (INRiM), 10135 Turin, Italy. ⁴Applied Quantum Systems, Felix-Bloch Institute for Solid-State Physics, Universität Leipzig, 04103 Leipzig, Germany. ⁵Laboratory for Ion Beam Interactions, Ruđer Bošković Institute, 10000 Zagreb, Croatia. ⁶Centre for Accelerator Science, Australian Nuclear Science and Technology Organisation, New Illawarra Road, Lucas Heights, NSW 2234, Australia. ✉email: jacopo.forneris@unito.it

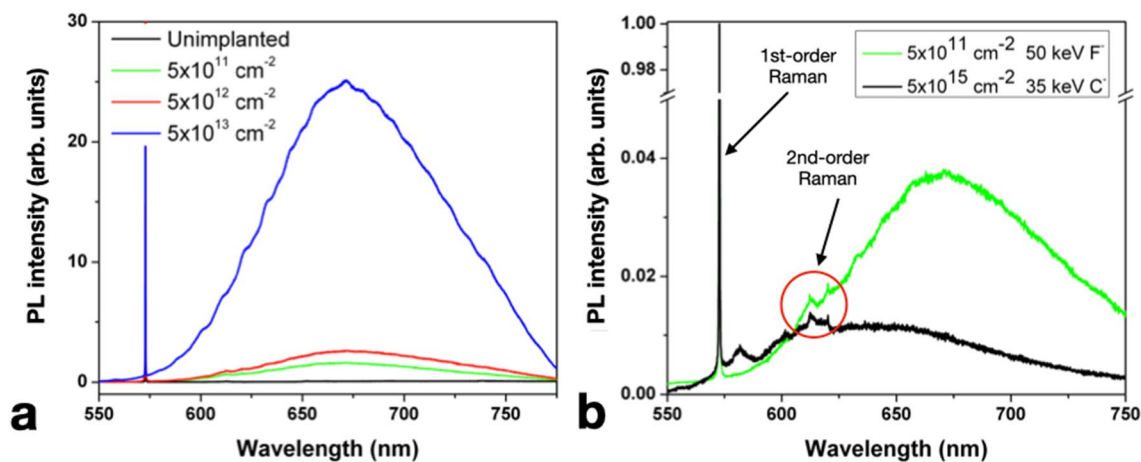


Figure 1. (a) PL spectra acquired under 532 nm laser excitation wavelength from regions implanted with different 5×10^{11} – 1×10^{13} cm^{-2} range. The PL spectrum of a pristine region of the sample is included for the sake of comparison (black line). (b) Comparison of the PL spectrum acquired from the region implanted with 5×10^{11} cm^{-2} 50 keV F-ion fluence (green line) with a sample region irradiated with 35 keV C⁻ ions at 5×10^{15} cm^{-2} fluence (black line). Both curves are normalized to the first-order Raman peak. The first-order and second-order Raman features of diamond are highlighted.

was then processed with a high-temperature thermal annealing (1200 °C, 4 h in vacuum at $\sim 10^{-6}$ mbar pressure) and a subsequent oxygen plasma treatment, with the purpose of minimizing the background fluorescence from surface contaminations. To compare the luminescence intensity of F-related ensembles with the well-known emission properties of the NV center, a nominally identical sample (Sample #2) was implanted at the ANSTO Centre for Accelerator Science with 10 keV N⁺ ions at a fluence of 10^{14} ions cm^{-2} . The implanted sample was then annealed at 950 °C for 2 h.

A preliminary PL characterization was performed using a Horiba Jobin–Yvon HR800 micro-Raman spectrometer equipped with a CW excitation laser at 532 nm wavelength.

Temperature-dependent PL measurements were performed using a custom-made cryogenic single-photon confocal microscope exploiting a closed-cycle optical cryostat operating in the 4–300 K temperature range. Optical excitation was provided through a $100\times$ air objective (0.85 NA) by a set of CW laser diodes with emission wavelengths of 405 nm, 488 nm and 520 nm. A suitable set of optical filters enabled the detection of PL emission at wavelengths larger than 550 nm. The PL spectra were acquired using a single-grating monochromator (1200 grooves mm^{-1} , 600 nm blaze) fiber-coupled to a Si-single-photon detector operating in Geiger mode. The spectral resolution of the apparatus was estimated to be ≤ 4 nm.

Results

PL emission at room temperature. Ensemble PL spectra acquired at room temperature are presented in Fig. 1 for different F implantation fluences.

The emission spectra reported in Fig. 1a were acquired from the implanted regions under 532 nm laser excitation (26.2 mW laser power) and exhibit a broad, intense and apparently unstructured PL band in the 600–800 nm spectral region (fluorine-related band, FB1, in the following), with a maximum centered at ~ 670 nm. Although not particularly characteristic in its spectral features, the observation of this band is consistent with what reported in Ref.²⁴ under 488 nm excitation, where a broad emission band in the 590–800 nm was formed upon F implantation at a 5×10^{14} cm^{-2} ion fluence and a subsequent thermal annealing at 1600 °C.

It is worth mentioning that the FB1 band is partially spectrally overlapping with the emission of the NV⁰ and NV⁻ center in diamond (i.e. PL bands in the 575–650, and 638–750 nm range, respectively, typically observed together in ensemble PL spectra⁴).

In order to benchmark the PL intensity of the F-related emission with respect to the one from NV centers, the photon count rate of the region implanted at 1×10^{13} cm^{-2} fluence was compared with that of Sample #2 (10 keV N⁺ implantation at 1×10^{14} cm^{-2} fluence) under the same experimental conditions (i.e.: 488 nm laser excitation at 2 mW optical power, long-pass 500 nm spectral filtering, and 488 nm and 520 nm notch filters to remove the laser line and the first-order Raman scattering).

Despite the F ion implantation fluence being 10 times smaller, the measured ensemble PL emission intensity from F-related centers of 5.4 Mcps was ~ 1.7 times higher with respect to what measured (3.2 Mcps) from the NV-centers ensemble. It is worth stressing that this result cannot be explicitly related to the brightness of individual F-related centers, since the efficiency in the formation of the active optical complex has yet to be determined. In this sense, the more intense PL emission at the ensemble level might be also caused by a higher formation efficiency with respect to the NV center. A direct comparison of the formation efficiency for the two types of color centers could not be performed, due to the fact that the dependence of the NV-ensemble PL emission intensity from the N⁺ implantation fluence is close to saturation at the considered value of 1×10^{14} cm^{-2} ²⁵. If the PL emission intensities from ensembles of both types are assumed to have reached a saturation with respect to

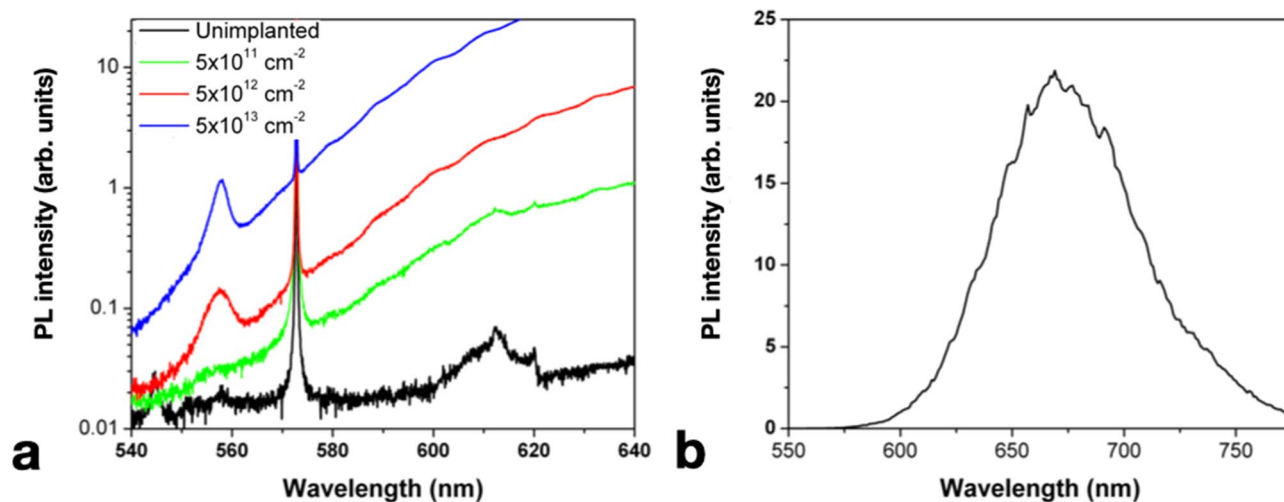


Figure 2. (a) Inset of Fig. 1a in the 540–660 nm spectral range. The axes are rescaled to highlight the PL emission peak at 558 nm. (b) PL spectrum acquired under 520 nm laser excitation from a sample region implanted with 1.47 MeV F^{2+} ions at $1 \times 10^{13} \text{ cm}^{-2}$ fluence.

irradiation fluence, then F-related centers would be estimated to be $5.4/3.2 \cong 1.7$ times brighter than NV centers. In the opposite case, if a full linear dependence of the ensemble PL emission intensity from ion irradiation fluence can still be assumed for both types of color centers, then the different fluence values should be taken into account, leading to a ~ 15 brightness increase estimation. Realistically, the most accurate estimation of the brightness increase can be assumed to be comprised between these boundary values. It is worth remarking that the higher PL emission intensity from the F-related ensemble is in line with the observation in Ref.²⁶ on the increased conversion efficiency of NV centers in N-implanted diamond upon the introduction of dopants with high-electron affinity such as S, O. According to this scheme, the optical activation of defects based on halogen impurities might follow a similar thermodynamic pathway.

In addition to the above discussion, to further rule out the possibility that the observed spectral feature can be attributed to NV-related emission, a pristine region of the same sample was irradiated with C^- ions at 35 keV energy ($5 \times 10^{15} \text{ cm}^{-2}$ fluence) and processed alongside the F-implanted region with the same annealing parameters. The PL spectrum from this test area, acquired under the same excitation conditions, is reported in Fig. 1b for the sake of comparison. It displays a significantly weaker band centered at 640 nm, whose intensity is comparable with the second-order Raman scattering of diamond observed at $\sim 620 \text{ nm}$ (corresponding to a 2664 cm^{-1} Raman shift), while not exhibiting any features similar to those observed for the FB1 band. This observation is indicative of the fact that the FB1 band is neither related to the formation of NV centers upon the introduction of lattice vacancies in a N-containing diamond substrate, nor to generic ion-induced structural damage.

In addition, the substantial increase (Fig. 1a) of the FB1 intensity at increasing F implantation fluences supports our attribution of this spectral feature to a stable F-containing defect in the diamond lattice.

Figure 2a displays a zoom-in in the 540–640 nm spectral range of the PL data reported in Fig. 1a. A weak PL peak at 558 nm appears in the regions implanted with F ions at fluences higher than $5 \times 10^{12} \text{ cm}^{-2}$. This peak was consistently observed in all of the room-temperature measurements performed on the F-implanted regions, while being absent from the test spectrum reported in Fig. 1b. While the peak position might be compatible with a 557 nm feature observed in cathodoluminescence from electron-irradiated diamonds that was previously attributed to an interstitial-type defect (ITD in the following)^{19,27}, a different interpretation is suggested by the persistence of the peak upon 1200 °C annealing (ITD is reported to anneal out at 700 °C²⁸). Furthermore, it is worth remarking that this spectral feature was not reported in a previous PL characterization of C-implanted diamond²⁹, and analogously has not been observed in our measurements in nominally identical samples implanted with a wide range of different ion species. Based on these considerations, a tentative attribution of the 558 nm line as related to an F-containing defect is made, although its relationship with the FB1 band is unclear on the basis of the available dataset.

Finally, Fig. 2b shows a PL spectrum acquired under 520 nm laser excitation (5.6 mW power, 565 nm long-pass filter) from the region implanted with 1.47 MeV F^{2+} ions at $1 \times 10^{13} \text{ cm}^{-2}$ fluence. Since the spectrum was acquired with the cryogenic single-photon confocal microscope rather than with the micro-Raman spectrometer, the PL intensity scale cannot be quantitatively compared with that of the previously discussed measurements. However, it is worth noting that Fig. 2b displays the same spectral features reported in Fig. 1a. This observation further corroborates the attribution of the emission spectrum to a F-containing lattice defect, and indicates that such optical center can be fabricated upon the implantation of fluorine ions of both keV and MeV energies (possibly with different creation yields, whose investigation is beyond the scope of this work), thus ruling out its possible attribution to intrinsic lattice defects related to high-energy irradiation effects.

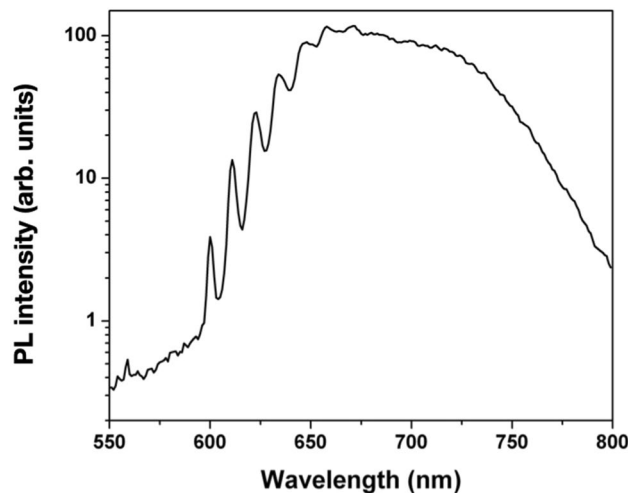


Figure 3. PL spectrum acquired at 4.5 K temperature under 488 nm laser excitation from the region of sample #1 implanted with at $5 \times 10^{13} \text{ cm}^{-2}$ fluence.

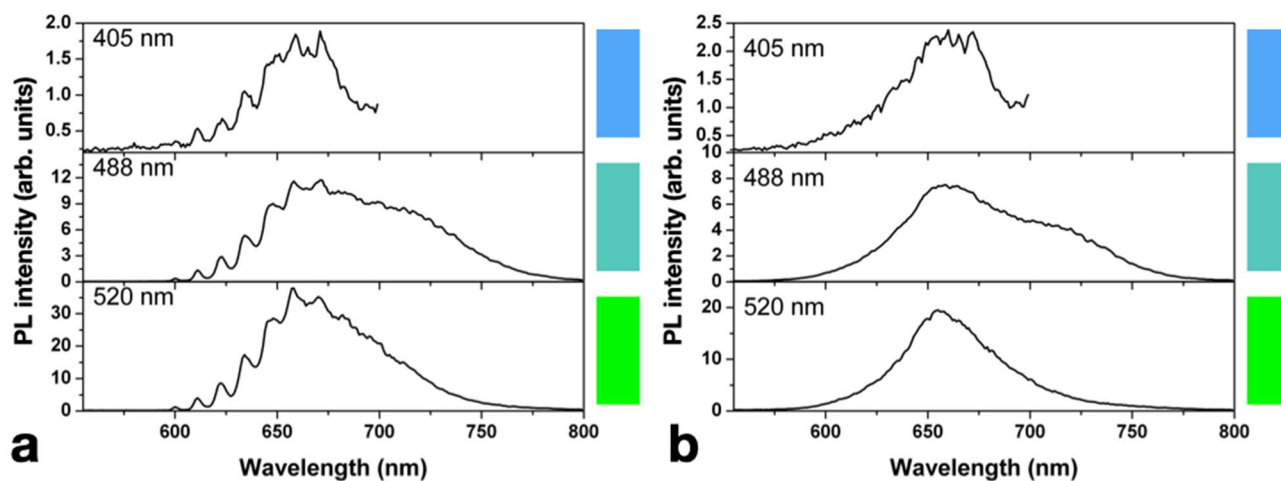


Figure 4. Ensemble PL spectra acquired at 4.5 K (a) and room temperature (b) from the region of sample #1 implanted at a fluence of $5 \times 10^{13} \text{ cm}^{-2}$ under different excitation wavelengths.

PL emission at variable temperatures. In order to gain a deeper insight into the spectral features of F-related color centers with respect to the aforementioned results and the previous report in Ref.²⁴, low-temperature PL measurements were performed at different excitation wavelengths. Figure 3 displays an ensemble PL spectrum acquired at 4.5 K under 488 nm excitation (3.6 mW laser power) from a region implanted at $5 \times 10^{13} \text{ cm}^{-2}$ fluence. At the reported temperature, the FB1 band reveals an articulated structure of different emission lines, the most prominent being located at 600, 611, 623, 634, 647, 658 and 671 nm. The linewidth estimation is limited by the spectral resolution ($\sim 4 \text{ nm}$) of the measurement system. In Fig. 4, PL spectra acquired from the same region both at 4.5 K and at room temperature are reported for different laser excitation wavelengths, including 405 nm (10 mW laser power) and 520 nm (2.4 mW). It is worth noting that the spectra acquired using the 405 nm laser were limited to the 500–700 nm spectral range due to the luminescence of optical elements employed in the confocal microscopy setup at higher wavelengths. The persistence of the emission lines at the same wavelengths under different excitation sources indicates that they cannot be attributed to Raman scattering. Furthermore, they can hardly be attributed to any interference process due to multiple internal reflections within the irradiated sample, firstly because they are visibly temperature-dependent, and most importantly because (differently from what is reported in Ref.³⁰) the implantation fluence is low enough to avoid the presence of a reflective layer below the sample surface. Within a $\sim 4 \text{ nm}$ limit due to the spectral resolution of the experimental apparatus, all of the aforementioned lines are uniformly spaced in energy of $\Delta E = (36 \pm 5) \text{ meV}$. If the 600 nm emission line corresponds, as assumed here, to the zero-phonon line (ZPL) of the F-related center, such energy shift value is compatible with an electron–phonon coupling, as it falls in the energy range (10–100 meV) related to quasi-local vibrations¹⁹.

Remarkably, the 558 nm line reported in Fig. 2a is also visible in Fig. 3, although its relative intensity with respect to the FB1 band maximum is further decreased with respect to room-temperature conditions. Such

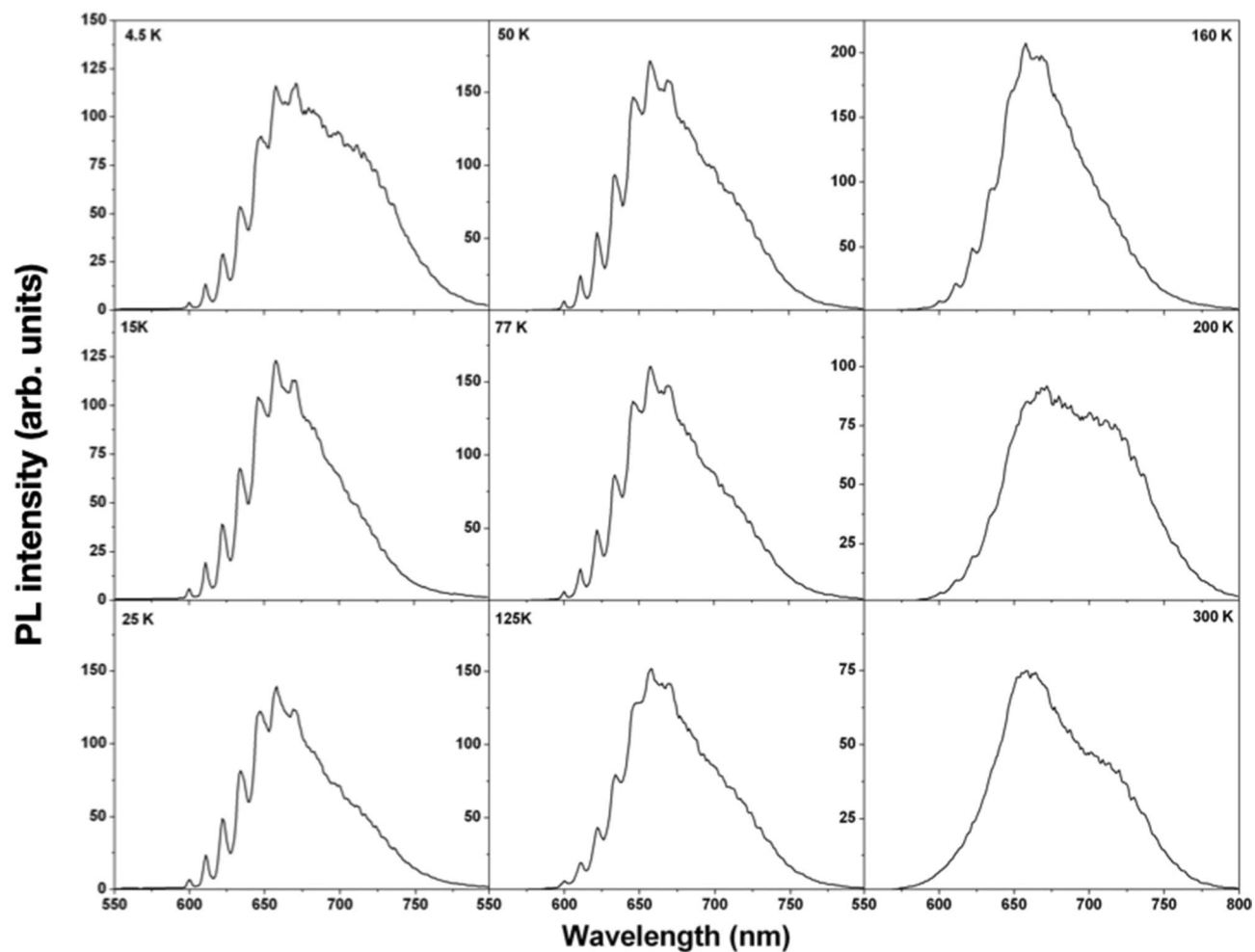


Figure 5. Ensemble PL emission from the region of sample #1 implanted at a fluence of $5 \times 10^{13} \text{ cm}^{-2}$ under 488 nm excitation as a function of temperature.

observation is indicative of the fact that the 558 nm emission can hardly be attributed to the ZPL of the FB1 band. This interpretation is further supported by the 155 meV energy separation with respect to its closest emission line at 600 nm. Therefore, the available experimental data are not sufficient to justify any reasonable attribution of the observed peak.

While no significant differences were observed among the PL peaks reported in Fig. 4, a comparison among the spectra reveals an additional emission band (FB2 in the following), which is visible (both at 4.5 K and 300 K) under 488 nm excitation only. This component appears as a second band centered at ~ 710 nm, not observed in the previous report on F-implanted diamond²⁴. The emergence of the FB2 band cannot be determined under 405 nm excitation as it lies outside of the available spectral range. If confirmed, its observation could lead to the attribution of FB1 and FB2 as different charge states of the same defect, in a similar fashion to the well-established interpretation of the emission bands of the neutral and negative charge states of the nitrogen-vacancy complex. In this case, FB2 would be related to a higher excitation energy (> 2.39 eV) with respect to FB1 despite resulting a lower photon energy. This might indicate the presence of indirect transitions or non-radiative processes involved in the luminescence mechanism, to be further assessed at the single-photon emitter level.

Figure 5 shows the PL spectra at various temperatures in the 4.5–300 K temperature range, under 488 nm excitation. The assessment of a trend in the relative intensity of the FB1 and FB2 bands was not possible due to slightly different focusing conditions. Nevertheless, the progressive broadening of the set of lines in the 600–670 nm range is clearly visible up to temperatures as high as 160 K, thus providing a further confirmation of their attribution as phonon sidebands of the 600 nm ZPL emission. Conversely, the absence of any distinguishable internal structure of the FB2 band even at 4.5 K temperature cannot be understood without a specific interpretative model, and thus will require further investigations.

Discussion and conclusions

In this work we reported on the fabrication by means of ion beam implantation and thermal annealing of a new class of color centers based on F impurities. The ensemble PL characterization showed several peculiar spectral features that, to the best of the authors' knowledge, were not reported so far at the state of the art, namely: a weak

emission peak at 558 nm, two bands centered at ~ 670 nm (FB1) and ~ 710 nm (FB2), the latter being visible under 488 nm excitation but not under 520 nm. At cryogenic temperatures, the FB1 band exhibited an articulated structure of separate emission lines, whose arrangement is compatible with the attribution of the 600 nm spectral features to the ZPL emission of the center, coupled to a set of six phonon replica spaced by a (36 ± 5) meV energy attributed to quasi-local vibrations. The weak 558 nm emission could not be related to the FB1, nonetheless it is not implausible that it originates from a different F-containing lattice defect.

The results discussed in this work, although limited to the study of ensembles of emitters, offer the first extensive characterization of F-related defects, thus confirming the claim on their optical activity presented in Ref.²⁴, where their characterization at the single-photon emitter level was challenging due to the strong similarity in both the spectral signatures and the excited state radiative lifetime with respect to those of the NV center⁴. A further study will be beneficial to assess the photoemission dynamics of the center and its brightness for potential use as single-photon source. A systematic investigation on individual centers will also be necessary in order to clarify the attribution of the 558 nm emission line and the nature of the FB2 band.

Preliminary *ab initio* simulations by J.P Goss and colleagues identified a stable neutral charge state of the fluorine-vacancy (F-V) complex with a ground state C_{2v} symmetry³¹. The evidence collected in this report leads to attribute the luminescence in F-implanted diamond to such complex. While the afore-mentioned work was not aimed at the identification of the center, the transitions from positive (neutral) to neutral (negative) charge states were calculated as $E_{0/+} = 3.0$ eV and $E_{-/0} = 1.9$ eV, respectively. The experimental observation of a significant decrease in the FB1 PL emission under 405 nm laser (~ 3.07 eV) with respect to higher excitation wavelengths might be compatible with the transition of the defect between two different charge states. In particular, the FB1 band might be attributed to its neutral charge state. This interpretation might be supported by future refined numerical simulations of the optical transitions of the defect, as well as by the observation of different spectral features under > 650 nm excitation wavelength (1.9 eV), at which the transition to the negative charge state is predicted to occur. On the other hand, such model does not suggest an interpretation for the FB2 band, which was observed under 488 nm excitation only.

The observation of optical activity from a F-V defect in diamond might also unveil further appealing practical applications in quantum technologies^{4–9,32} and in particular in quantum sensing and quantum computation, since the theoretical model in Ref.³¹ suggests a ground state electronic spin configuration similar to that of the NV center ($S = 1/2$, and $S = 1$ for neutrally- and negatively-charged impurity-vacancy defects, respectively). If confirmed by EPR experiments, such property could pave the way to the utilization of F-related centers in diamond for quantum information processing applications, taking advantage of the non-zero nuclear spin of the naturally occurring ¹⁹F for hyperfine interactions for defects control and coupling³¹.

Received: 31 July 2020; Accepted: 5 November 2020

Published online: 09 December 2020

References

- Schröder, T. *et al.* Quantum nanophotonics in diamond. *J. Opt. Soc. Am. B* **33**(4), B65 (2016).
- Aharonovic, I., Englund, D. & Toth, M. Solid-state single-photon emitter. *Nat. Photonics* **10**, 631 (2016).
- Chen, D., Zheludev, N. & Gao, W. Building blocks for quantum network based on group-iv split-vacancy centers in diamond. *Adv. Quantum Technol.* **3**, 1900069 (2020).
- Doherty, M. W. *et al.* The nitrogen-vacancy colour centre in diamond. *Phys. Rep.* **528**, 1 (2013).
- Staudacher, T. *et al.* Nuclear magnetic resonance spectroscopy on a (5-nanometer) 3 sample volume. *Science* **339**, 561 (2013).
- Dolde, F. *et al.* Nanoscale detection of a single fundamental charge in ambient conditions using the NV– center in diamond. *Phys. Rev. Lett.* **112**, 097603 (2014).
- Sipahigil, A. *et al.* Quantum interference of single photons from remote nitrogen-vacancy centers in diamond. *Phys. Rev. Lett.* **108**, 143601 (2012).
- Le Sage, D. *et al.* Efficient photon detection from color centers in a diamond optical waveguide. *Phys. Rev. B* **85**, 121202 (2012).
- Schirhagl, R., Chang, K., Loretz, M. & Degen, C. L. Nitrogen-vacancy centers in diamond: nanoscale sensors for physics and biology. *Ann. Rev. Phys. Chem.* **65**, 83 (2014).
- Bradac, C., Gao, W., Forneris, J., Trusheim, M. E. & Aharonovich, I. Quantum nanophotonics with group IV defects in diamond. *Nat. Commun.* **10**, 5625 (2019).
- Wang, C., Kurtsiefer, C., Weinfurter, H. & Burchard, B. Single photon emission from SiV centres in diamond produced by ion implantation. *J. Phys. B* **39**, 37 (2006).
- Müller, T. *et al.* Optical signatures of silicon-vacancy spins in diamond. *Nat. Commun.* **5**, 3328 (2014).
- Palyanov, Y. N., Kupriyanov, I. N., Borzdov, Y. M. & Surovtsev, N. V. Germanium: a new catalyst for diamond synthesis and a new optically active impurity in diamond. *Sci. Rep.* **5**, 14789 (2015).
- Iwasaki, T. *et al.* Germanium-vacancy single color centers in diamond. *Sci. Rep.* **5**, 12882 (2015).
- Ditalia Tchernij, S. *et al.* Single-photon-emitting optical centers in diamond fabricated upon sn implantation. *ACS Photonics* **4**, 2580 (2017).
- Iwasaki, T. *et al.* Tin-vacancy quantum emitters in diamond. *Phys. Rev. Lett.* **119**, 253601 (2017).
- Ditalia Tchernij, S. *et al.* Single-photon emitters in lead-implanted single-crystal diamond. *ACS Photonics* **5**, 4864 (2018).
- Trusheim, M. *et al.* Lead-related quantum emitters in diamond. *Phys. Rev. B* **99**, 075430 (2019).
- Zaitsev, A. M. *Optical Properties of Diamond: Data Handbook* (Springer, Berlin, 2001).
- Forneris, J. *et al.* Creation and characterization of He-related color centers in diamond. *J. Lumin.* **179**, 59 (2016).
- Sandstrom, R. *et al.* Optical properties of implanted Xe color centers in diamond. *Optics Commun.* **411**, 182–186 (2018).
- Pezzagna, S., Rogalla, D., Wildanger, D., Meijer, J. & Zaitsev, A. Creation and nature of optical centres in diamond for single-photon emission—overview and critical remarks. *New J. Phys.* **13**, 035024 (2011).
- Orwa, J. *et al.* Fabrication of single optical centres in diamond—a review. *J. Lumin.* **130**, 1646 (2010).
- Lühmann, T. *et al.* Screening and engineering of colour centres in diamond. *J. Phys. D Appl. Phys.* **51**, 483002 (2018).
- Pezzagna, S., Naydenov, B., Jelezko, F., Wrachtrup, J. & Meijer, J. Creation efficiency of nitrogen-vacancy centres in diamond. *New J. Phys.* **12**, 065017 (2010).
- Lühmann, T., John, R., Wunderlich, R., Meijer, J. & Pezzagna, S. Coulomb-driven single defect engineering for scalable qubits and spin sensors in diamond. *Nat. Commun.* **10**, 4956 (2019).

27. Gatto Monticone, D. *et al.* Native NIR-emitting single colour centres in CVD diamond. *New J. Phys.* **16**, 053005 (2014).
28. Steeds, J. W., Davis, T. J., Charles, S. J., Hayes, J. M. & Butler, J. E. 3H luminescence in electron-irradiated diamond samples and its relationship to self-interstitials. *Diam. Relat. Mater.* **8**, 1847 (1999).
29. Forneris, J. *et al.* Electrical control of deep NV centers in diamond by means of sub-superficial graphitic micro-electrodes. *Carbon* **113**, 76–86 (2017).
30. Olivero, P. *et al.* Characterization of three-dimensional microstructures in single-crystal diamond. *Diam. Relat. Mater.* **15**, 1614 (2006).
31. Goss, J. P., Briddon, P. R., Rayson, M. J., Sque, S. J. & Jones, R. Vacancy-impurity complexes and limitations for implantation doping of diamond. *Phys. Rev. B* **72**, 035214 (2005).
32. Petrini, G., Moreva, E., Bernardi, E., Traina, P., Tomagra, G., Carabelli, V., Degiovanni, I. P. & Genovese, M., Is a quantum biosensing revolution approaching? Perspectives in NV-assisted current and thermal biosensing in living cells. *Adv. Quantum Technol.* 2000066 (2020).

Acknowledgements

This work was supported by the following projects: Coordinated Research Project “F11020” of the International Atomic Energy Agency (IAEA); Project “Piemonte Quantum Enabling Technologies” (PiQuET), funded by the Piemonte Region within the “Infra-P” scheme (POR-FESR 2014-2020 program of the European Union); “Departments of Excellence” (L. 232/2016), funded by the Italian Ministry of Education, University and Research (MIUR); “Ex post funding of research” of the University of Torino funded by the “Compagnia di San Paolo”; FET OPEN Pathos. The project 17FUN06 (SIQUST) leading to this publication has received funding from the EMPIR programme co-financed by the Participating States and from the European Union’s Horizon 2020 research and innovation programme. T.L., S.P and J.M. acknowledge the support of the ASTERIQS program of the European Commission. S.D.T. and J.F. gratefully acknowledge the EU RADIATE Project (proposal 19001744) for granting transnational access to the Laboratories of the Ruđer Bosković Institute.

Author contributions

J.F., P.O. M.G., S.D.T, designed the experiments. T.L., J.M. and S.P. performed keV F implantations; A.C., M.B., and Z.S., S.D.T performed MeV F ion implantations. Z.P. performed keV N implantations. F.S., P.A., F. P., E.C. contributed with post-implantation sample processing, room-temperature ensemble measurements, and micro-Raman photoluminescence spectroscopy. J. F., E.M. I.P.D., and P.T. developed a cryogenic confocal microscopy setup and acquired PL spectra at varying temperatures. J.F., S.D.T, P.O. performed the analyses and wrote the manuscript. All authors contributed to revise the manuscript.

Competing interests

The authors declare no competing interests.

Additional information

Correspondence and requests for materials should be addressed to J.F.

Reprints and permissions information is available at www.nature.com/reprints.

Publisher’s note Springer Nature remains neutral with regard to jurisdictional claims in published maps and institutional affiliations.



Open Access This article is licensed under a Creative Commons Attribution 4.0 International License, which permits use, sharing, adaptation, distribution and reproduction in any medium or format, as long as you give appropriate credit to the original author(s) and the source, provide a link to the Creative Commons licence, and indicate if changes were made. The images or other third party material in this article are included in the article’s Creative Commons licence, unless indicated otherwise in a credit line to the material. If material is not included in the article’s Creative Commons licence and your intended use is not permitted by statutory regulation or exceeds the permitted use, you will need to obtain permission directly from the copyright holder. To view a copy of this licence, visit <http://creativecommons.org/licenses/by/4.0/>.

© The Author(s) 2020